

Neutron Scattering for Biology

T.A. Harroun, G.D. Wignall, J. Katsaras

1.1 Introduction

The structure and dynamics of a specimen can be determined by measuring the changes in energy and momentum of neutrons scattered by the sample. For biological materials, the structures of interest may be complex molecular structures, membranes, crystal lattices of macromolecules (e.g., proteins), micellar dispersions, or various kinds of aggregates. These soft materials may exhibit various modes of motion, such as low-energy vibrations, undulations or diffusion.

Neutrons are non-charged particles that penetrate deeply into matter. Neutrons are isotope-sensitive, and as they possess a magnetic moment, scatter from magnetic structures. Neutron scattering can often reveal aspects of structure and dynamics that are difficult to observe by other probes, including X-ray diffraction, nuclear magnetic resonance, optical microscopy, and various spectroscopies. It is particularly powerful for the study of biologically relevant materials which often contain hydrogen atoms and must be held in precise conditions of pH, temperature, pressure, and/or hydration in order to reveal the behaviors of interest.

Neutron scattering is practiced at facilities possessing reactor-based and accelerator-based neutron sources, and to which researchers travel to undertake their scattering experiments with the help of local scientific and technical expertise. Compared to traditional “hard” materials, in biologically relevant materials the characteristic length-scales are larger and the energy levels are lower. As such, additional neutron scattering measurements are possible if the reactor or accelerator-based source includes a cold moderator that emits a large proportion of long wavelength, lower velocity neutrons, which are better suited to the typical structures and dynamics found in bio-materials.

This chapter will follow neutrons from their production in a fission or spallation event, into the specimen where they scatter and are subsequently detected in a way that discriminates changes in momentum and energy. The advantages of using neutron scattering for problems in biology will be outlined.

However, details of specific instruments and data analysis for the associated scattering methods will be left to subsequent chapters.

1.2 Production of Neutrons

The neutron is a neutral, subatomic, elementary particle that had been postulated by Rutherford, and discovered in 1932 by James Chadwick [1, 2]. It is found in all atomic nuclei except hydrogen (^1H), has a mass similar to the proton, a nuclear spin of $1/2$, and a magnetic moment [3]. Neutron beams with intensities suitable for scattering experiments are presently being produced either by nuclear reactors (Fig. 1.1), where the fission of uranium nuclei results in neutrons of energies between 0.5 and 3 MeV [4], or by spallation sources (Fig. 1.2), where accelerated subatomic particles (e.g., protons) strike a heavy metal target (e.g., tungsten or lead), expelling neutrons from the target nuclei [5].

In Canada, for example, the 125 MW National Research Universal (NRU) reactor, located at Chalk River Laboratories, has a peak thermal flux of

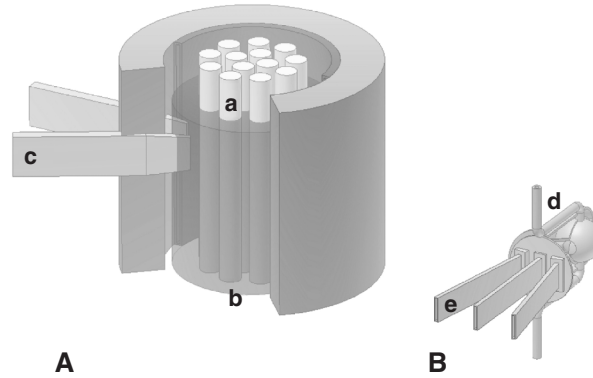


Fig. 1.1. Schematic of a nuclear reactor that produces thermal neutrons. Fuel rods (a) contain ^{235}U atoms which when they encounter moderated neutrons undergo fission producing ~ 2.5 high-energy neutrons/ ^{235}U atom. The probability of a fast (high energy) neutron interacting with a ^{235}U atom is small. To sustain the chain reaction, neutrons must be slowed down or thermalized by passing through a moderator. In practice, moderators such as H_2O , D_2O , graphite, or beryllium are used, filling the space in the reactor core around the fuel rods. For reasons of cost, H_2O is the most commonly used moderator (b) Thermal neutrons with a peak flux centered at $\sim 1.2 \text{ \AA}$ can either be extracted directly from the reactor via a beam tube (c) or can be furthered slowed down by interaction with another, colder moderator, for example, a vessel of liquid hydrogen (d) These cold neutrons, with their Maxwellian distribution shifted toward lower energies, can be transported over many meters to the various spectrometers by ^{58}Ni -coated optically flat glass surfaces (e) through a process known as total external reflection

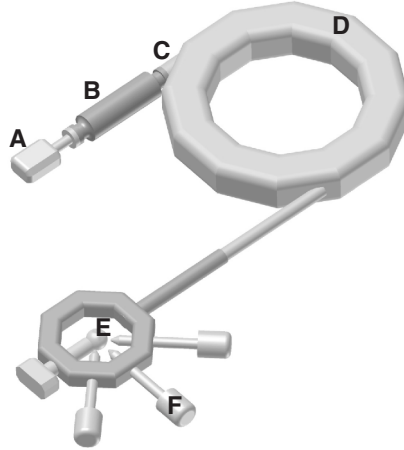


Fig. 1.2. Schematic of the Spallation Neutron Source (SNS) presently under construction at Oak Ridge National Laboratory. (a) H^- ions produced by an ion source are accelerated to 2.5 MeV (b) the H^- ion beam is then delivered to a Linac further accelerating the 2.5 MeV H^- ion beam to 1 GeV (c) prior to delivery from the Linac to the accumulator ring, H^- ions are stripped of all of their electrons by a stripper foil resulting in H^+ ions (d) these H^+ ions are bunched and intensified by the accumulator ring for delivery to the (e) liquid mercury target where a nuclear reaction takes place creating spallation neutrons for use at various spectrometers (f) the duration of the SNS proton pulse is 10^{-6} s and the repetition rate is 60 Hz. Not unlike reactor-based neutrons, spallation neutrons are moderated by either water or a liquid hydrogen source, giving rise to thermal or cold neutrons, respectively. The SNS chose mercury as the target for the proton pulses for the following reasons: (i) Unlike solid materials, liquid mercury does not experience radiation damage. (ii) Mercury is a high atomic number material resulting in many spallation neutrons ($\sim 20\text{--}30$ neutrons/mercury atom). (iii) Compared to a solid target, a liquid target at room temperature better dissipates heat and withstands shock effects

3×10^{14} neutrons $\text{cm}^{-2} \text{ s}^{-1}$. Fast MeV neutrons are produced from fission of ^{235}U atoms which are in turn thermalized, through successive collisions with deuterium atoms in a heavy water moderator at room temperature, to an average energy of ~ 0.025 eV. Neutron beams exiting the reactor have a Maxwellian distribution of energy, [4] and are usually monochromated using a crystal monochromator, and then used to study a variety of condensed matter.

For a thermal neutron reactor, such as the Institut Laue-Langevin (ILL, Grenoble, France) the Maxwell spectrum peak is centered at $\sim 1 \text{ \AA}$ due to a 300 K D_2O moderator [6]. However, the peak of the spectrum can be shifted to higher energies (or shorter wavelengths) by allowing the thermal neutrons to equilibrate with a “hot source”, or shifted to lower energies with the use

of a “cold source”. For example, the ILL uses a self-heating graphite block hot-source at 2400 K to produce higher energy neutrons, [7] while the reactor at the National Institute of Standards and Technology (NIST, Gaithersburg, Maryland) produces lower energy cold neutrons by passing thermal neutrons through a vessel filled with liquid hydrogen at 40 K [8]. Similarly, a supercritical hydrogen moderator at 20 K is currently being installed at the Oak Ridge National Laboratory (ORNL, Oak Ridge, Tennessee) High Flux Isotope Reactor (HFIR) that will feed a suite of instruments, including a 35 m small-angle neutron scattering facility optimized for the study of biological systems (see contribution by Krueger and Wignall this volume) [9].

Presently, the heavy-water moderated ILL and light-water moderated ORNL reactors produce the highest flux neutron beams, operating at a thermal power of 58 and 85 MW, respectively. The peak core flux of both sources is $>10^{15}$ neutrons $\text{cm}^{-2} \text{s}^{-1}$. Since the ability to remove heat from the reactor core dictates the maximum power density, and thus the maximum neutron flux, it is unlikely that a reactor far exceeding the thermal flux characteristics of the ILL and ORNL high flux reactors will ever be constructed.

The notion of accelerator driven neutron sources dates back to the 1950s. In an accelerator-based pulsed neutron source, high energy subatomic particles, such as protons, are produced in a linear accelerator (Linac) [10–12]. These accelerated protons then impinge on a heavy metal target releasing neutrons from the nuclei of the target material. Since the Linac operation uses travelling electromagnetic waves, the arrival of the protons at the target are in pulsed bunches, and therefore the neutron beams produced are also pulsed. As with neutrons produced in a reactor, spallation neutrons have very high initial energies and must be slowed down from MeV to meV energies. However, their characteristic spectra differ considerably as the neutron spectrum from a spallation source contains both a high energy slowing component of incomplete thermalized neutrons, and a Maxwell distribution characteristic of the moderator temperature. Compared to reactor sources, the biggest advantage of spallation sources is that they create much less heat per neutron produced, translating into increased neutron fluxes. Nevertheless, since neutrons are produced in pulses, the time-averaged flux of even the most powerful pulsed source, that of ISIS (Oxford, UK), is less than that of a high flux reactor source (e.g., ILL). However, judicious use of time-of-flight techniques, which can utilize the many neutron wavelengths present in each pulse, can exploit the high brightness and can, for certain experiments, more than compensate for the time-averaged flux disadvantage.

The Spallation Neutron Source (SNS), presently being constructed at ORNL, will have a time-averaged flux comparable to a high-flux reactor but each pulse will contain neutron intensities between 50 and 100 times greater than the ILL or ORNL reactor-based sources. Moreover, the intense short-pulse neutron beams produced by accelerator-based neutron sources make it possible to perform time-of-flight experiments, and the study of kinetics and dynamics of various systems.

1.3 Elements of Neutron Scattering Theory

1.3.1 Properties of Neutrons

X-rays interact with charged subparticles of an atom, primarily with electrons [13]. On the other hand, neutrons, as mentioned previously, are non-charged subatomic particles having a mass (m) of 1.0087 atomic mass units (1.675×10^{-27} kg), spin of 1/2, and a magnetic moment (μ_n) of -1.9132 nuclear magnetons [6]. These properties of the neutron give rise to two principal modes of interaction which are different from those of X-rays.

As neutrons are zero charge particles, their interaction with matter, both nuclear and magnetic, is short ranged. As a result of this small interaction probability, neutrons can penetrate deep into condensed matter. Moreover, the interaction between the neutron and atomic nuclei involve complex nuclear interactions between the nuclear spins and magnetic moments. For this reason, there is no general trend throughout the periodic table of an atom's ability to scatter neutrons. This is quite unlike the X-ray atomic scattering factor which increases with atomic number [13, 14]. In addition, different isotopes of the same element may have very different abilities to scatter neutrons. This concept of a difference in scattering power, or *contrast*, between various components in a sample as a result of the different scattering properties of the various elements (particularly ^1H and ^2H) is the core principle of neutron scattering, and from which biology greatly benefits [14–16].

The second mode of interaction is the magnetic dipole interaction between the magnetic moments associated with unpaired electron spins in magnetic samples and the nuclear magnetic moment of the neutron. This type of neutron–atom interaction is of limited use to biology, and as such, for the purposes of this chapter only nuclear scattering will be considered. It should be noted that the interaction between the magnetic field of the X-ray and the orbital magnetic moments of the electron is not zero. However, compared to charge scattering, X-ray magnetic scattering is weak [13].

1.3.2 Energy and Momentum Transfer

In a scattering experiment the neutron undergoes a change in momentum after interacting with the sample. This means the neutron has a change in direction and/or velocity. The neutron's momentum is given by $\mathbf{p} = \hbar\mathbf{k}$, where $\hbar = h/2\pi$ is Planck's constant and \mathbf{k} is the neutron wave vector, $|\mathbf{k}| = 2\pi/\lambda$. The wavelength, λ , of a neutron is given by

$$\frac{h^2}{2m\lambda^2} = 2k_{\text{B}}T, \quad (1.1)$$

where k_{B} is Boltzmann's constant and T is the neutron moderator temperature.

The momentum change can be described by a momentum transfer vector or the *scattering vector*, \mathbf{Q} , and is defined as the vector difference between the incoming and scattered wave vectors,

$$\mathbf{Q} = \mathbf{k}_0 - \mathbf{k}_1, \quad (1.2)$$

where \mathbf{k}_0 and \mathbf{k}_1 are the incident and scattered wave vectors, respectively (Fig. 1.3). The change in the neutron's momentum is given by $\hbar\mathbf{Q}$.

Besides a change in direction, the magnitude of \mathbf{k} can also change as energy between the incident neutron and the sample are exchanged. The law of energy conservation can be expressed as

$$E = E_0 - E_1 = \hbar^2 \frac{\mathbf{k}_0^2}{2m} - \hbar^2 \frac{\mathbf{k}_1^2}{2m} = \hbar\omega, \quad (1.3)$$

where E is the energy gained or lost by the neutron. Any process whereby the neutron is scattered from \mathbf{k}_0 to \mathbf{k}_1 is therefore associated with \mathbf{Q} and E .

1.3.3 Diffraction

Scattering is totally *elastic* when $E = 0$. In this case, from Eq. 1.3 we must have $|\mathbf{k}_1| = |\mathbf{k}_0|$ and as such, from Eq. 1.2 we get $|\mathbf{Q}| = 2\mathbf{k}_0 \sin \theta$. For crystalline materials Bragg peaks appear at values \mathbf{Q} equal to the reciprocal lattice spacing:

$$|\mathbf{Q}| = \frac{2\pi}{d}, \quad (1.4)$$

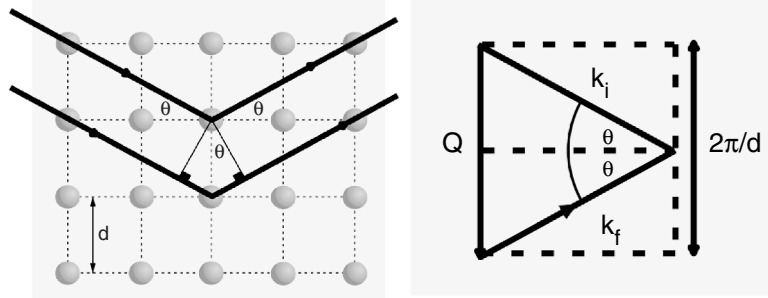


Fig. 1.3. Neutrons strike an array of atoms (green) from the left, and are scattered to the right. Horizontal planes of atoms are separated by distance d . Both the incident and diffracted neutron beams make an angle θ with respect to the planes of atoms (*left*). The change of the neutron's momentum, \mathbf{Q} , is given in Eq. 1.2 and is schematically represented schematically. In reciprocal space, when \mathbf{Q} points along the reciprocal lattice of spacing $2\pi/d$, the Bragg condition for diffraction is met, and constructive interference leads to a diffraction peak or so-called Bragg maximum (*right*)

where d is the characteristic spacing of a set of crystal planes. Since $\mathbf{k}_0 = 2\pi/\lambda$, carrying out the appropriate substitutions leads to the now familiar Bragg formula:

$$\lambda = 2d \sin \theta. \quad (1.5)$$

Simply stated, this is the condition of constructive interference of waves with incident angle θ on a set of equidistant planes separated by a distance d .

The measurement of truly elastic scattering requires that both the incident and scattered neutrons have the same wavelength, i.e., $|\mathbf{k}_1| = |\mathbf{k}_0|$. However, in practice this type of elastic scattering experiment, using an analyzer crystal to choose the appropriate energy scattered neutron, is seldom performed and the inelastic contribution ($E \neq 0$) is usually not removed.

1.3.4 Scattering Length and Cross-Section

Neutron, X-ray, and light scattering all involve interference phenomena between the wavelets scattered by different elements in the system. In the simple case of neutron scattering from a single, fixed nucleus, incident neutrons can be represented as a plane wave, $\psi_0 = \exp i\mathbf{k}_0 z$. The resulting scattered wave is a spherical wave, and is given by

$$\psi_1 = \frac{b}{r} e^{i\mathbf{k}_1 \cdot \mathbf{r}}, \quad (1.6)$$

where \mathbf{r} is the location of the detector from the nucleus. The quantity b has the dimensions of length, and is the measure of the scattering ability of the atomic nucleus. It may be regarded as a real and known constant for a given nucleus or isotope.

A typical experiment involves counting the number of neutrons scattered in a particular direction, and in this simple case, without regard of any changes in energy. If the distance from the detector to the nucleus is assumed to be large, so that the small solid angle $d\Omega$ subtended by the detector is well defined, we can then define the *differential cross-section* as

$$\frac{d\sigma}{d\Omega} = \frac{(\text{neutrons s}^{-1} \text{ scattered into } d\Omega)}{\Phi d\Omega}, \quad (1.7)$$

where Φ is the incident neutron flux (number of neutrons $\text{cm}^{-2} \text{s}^{-1}$). The *total scattering cross-section* is defined as the total number of neutrons scattered per second, normalized to the flux;

$$\sigma_s = \int \left(\frac{d\sigma}{d\Omega} \right) d\Omega, \quad (1.8)$$

where the integral is over all directions. For the single, fixed nucleus that we are considering, we can readily relate the total cross-section to b . If v is

the velocity of the incident neutrons, then the number of neutrons passing through an area dS s^{-1} is

$$vdS |\psi|^2 = vdS \frac{b^2}{r^2} = vb^2 d\Omega. \quad (1.9)$$

From the definition of a neutron cross-section,

$$\frac{d\sigma}{d\Omega} = \frac{vb^2 d\Omega}{\Phi d\Omega}, \quad (1.10)$$

where $\sigma_s = 4\pi b^2$ [17].

From the above it is obvious that σ_s has the dimensions of area. Moreover, the magnitude of b is typically of the order 10^{-12} cm, giving rise to the usual unit for cross-section, commonly known as the barn (1 barn = 10^{-24} cm²).¹ To a first approximation, the cross-section may be regarded as the effective area which the target nucleus presents to the incident beam of neutrons for the elastic scattering process and is usually referred-to as the *bound atom* cross-section, as the nucleus is considered fixed at the origin [18]. Where the atom is free to recoil, such as in the gaseous state, the *free atom* cross-section is applicable. The bound atom cross-section is generally relevant to biological studies which are virtually always conducted on samples of macroscopic dimensions in the solid or liquid state.

Neutrons are scattered isotropically from individual nuclei, whereas for X-ray scattering, the scattering originates in the electron cloud, which is very large compared to the X-ray wavelength. In the case of X-rays, the atomic form factors are Q -dependent. However, the variation in practice is small ($<1\%$ for $Q < 0.1 \text{ \AA}^{-1}$), and usually neglected in the small angle region. The Thompson scattering amplitude of a classical electron is $r_T = 0.282 \times 10^{-12}$ cm, so the X-ray scattering length of an atom, f , is proportional to the atomic number ($f = r_T Z$) and increases with the number of electrons/atom. For neutrons, values of b vary from isotope to isotope (Sect. 1.3.5). If the nucleus has a nonzero spin, it can interact with the neutron spin, and the total cross-section (σ_s) contains both, coherent and incoherent components.

1.3.5 Coherent and Incoherent Cross-Sections

Atomic nuclei are characterized by an incoherent and a coherent neutron scattering length b . The coherent scattering length is analogous to the atomic form factor in X-rays, f , while there is no X-ray analogue for the incoherent scattering length. For the purposes of this review, we will only consider the case where the nuclear moments of the material being probed with neutrons are completely disordered, giving rise to incoherent scattering.

¹The origin of the barn unit is thought to lie in the colloquialism “as big as a barn”, and was recommended in 1950 by the Joint Commission on Standards, Units and Constants of Radioactivity, because of its common usage in the USA.

When a neutron of spin $1/2$ encounters a single isotope with nuclear spin I , the spin of the neutron–nucleus system can assume two values, $I \pm 1/2$. The scattering lengths of the two systems are denoted by b^+ and b^- , and the number of spin states associated with each are $2(I + 1/2) + 1 = 2I + 2$ and $2(I - 1/2) + 1 = 2I$, respectively. The total number of states is $4I + 2$. If the neutrons are unpolarized and the nuclear spins are randomly oriented, each spin state has the same probability. Thus the frequency of the b^+ occurring is weighted by $(I + 1)/(2I + 1)$, and for b^- , $I/(2I + 1)$. The coherent cross-section for each isotope is given as $\sigma_c = 4\pi\bar{b}^2$, where \bar{b} represents the thermally averaged scattering length with $+$ and $-$ spin state populations. Similarly, the total scattering cross-section is given by $\sigma_s = 4\pi\bar{b}^2$. The average coherent scattering length is then given by

$$\bar{b} = \frac{1}{2I + 1} [(I + 1)b^+ + Ib^-], \quad (1.11)$$

$$\bar{b}^2 = \frac{1}{2I + 1} [(I + 1)(b^+)^2 + I(b^-)^2], \quad (1.12)$$

The difference between σ_s and σ_c is the incoherent scattering cross-section, σ_i .

If the isotope has no spin (e.g., ^{12}C), then $b^2 = \bar{b}^2 = \overline{b^2}$ and there is no incoherent scattering. Only the coherent scattering cross-section contains information on interference effects arising from spatial correlations of the nuclei in the system, in other words, the structure of the sample. The incoherent cross-section contains no structural information or interference effects, and forms an isotropic (flat) background which must be subtracted off from the raw data (e.g., see J. Krueger et al. this volume). The incoherent component of the scattering does, however, contain information on the motion of single atoms which may be investigated via by studying the changes in energy of the scattered beam (e.g., see contributions by Lechner et al., Doster, Sokolov et al. or Fitter in this volume).

While most of the atoms encountered in neutron scattering of biologically relevant materials are mainly coherent scatterers, such as carbon and oxygen, there is one important exception. In the case of hydrogen (^1H) the spin-up and spin-down scattering lengths have opposite sign ($b^+ = 1.080 \times 10^{-12}$ cm; $b^- = -4.737 \times 10^{-12}$ cm). Since $I = 1/2$ we then have σ_c , σ_i , and σ_s equal to 1.76×10^{-24} , 79.7×10^{-24} , and 81.5×10^{-24} cm², respectively.

Unlike neutrons, for photons there is no strict analog of incoherent scattering. X-ray Compton scattering is similar in that it contains no information on interference effects, i.e., the structure of the sample, and contributes a background to the coherent signal. However, to a good approximation this background goes to zero in the limit $Q \rightarrow 0$ and in X-ray studies, is usually neglected. Table 1.1 gives the cross-sections and scattering lengths for atoms commonly encountered in synthetic, natural and biomaterials.

The cross-sections given previously for hydrogen refer to bound protons and neglect inelastic effects arising from the interchange of energy with the

Table 1.1. Bound atom scattering lengths and cross-sections for typical elements in synthetic and natural biomaterials

atom	nucleus	b_c (10^{-12} cm)	σ_c (10^{-24} cm ²)	σ_i (10^{-24} cm ²)	σ_{abs}^a (10^{-24} cm ²)	$f_{\text{X-ray}}$ (10^{-12} cm)
hydrogen	¹ H	−0.374	1.76	79.7	0.33	0.28
deuterium	² H	0.667	5.59	2.01	0	0.28
carbon	¹² C	0.665	5.56	0	0	1.69
nitrogen	¹⁴ N	0.930	11.1	0	1.88	1.97
oxygen	¹⁶ O	0.580	4.23	0	0	2.25
fluorine	¹⁹ F	0.556	4.03	0	0	2.53
silicon	²⁸ Si	0.415	2.16	0	0.18	3.94
phosphorous	P ^b	0.513	3.31	0	0.17	4.22
chlorine	Cl ^b	0.958	11.53	5.9	33.6	4.74

^a Values of the absorption cross-section (σ_{abs}) are a function of wavelength and are given at $\lambda = 1.8 \text{ \AA}$. As $\sigma_{\text{abs}} \sim \lambda$, values at other wavelengths may be estimated by scaling by $\lambda/1.8$; $f_{\text{X-ray}}$ is given for $\theta = 0$

^b Values are an average over the natural abundance of the various isotopes

neutron. For coherent scattering, which is a collective effect arising from the interference of scattered waves over a large correlation volume, this approximation is reasonable, especially at low Q where recoil effects are small. However, for incoherent scattering, which depends on the uncorrelated motion of individual atoms, inelastic effects become increasingly important for long wavelength neutrons. In most biological systems, the atoms are not rigidly bound, so due to effects of torsion, rotation, and vibration, the scattering generally contains an inelastic component. This has two consequences: Firstly, the scattering, which in the center-of-mass system is elastic, may induce a change of energy of the neutron in the laboratory frame. This gives rise to inelastic scattering which contains information about the motion of atoms in the sample (e.g., see Lechner et al.). Secondly, the effective total scattering cross-section in the laboratory system is wavelength-dependent, an effect that is particularly important for ¹H-containing samples, where the transmission is a function of both the incident neutron energy and temperature. This effect is important for H₂O, a common solvent for biomaterials, and for which the total scattering cross-section at 20°C is given by $\log \sigma = 4.45 + 0.46 \log \lambda$, where σ is expressed in barns [19]. For further discussion of such inelastic effects, see contribution by S. Krueger et al.

1.4 Neutron Diffraction and Contrast

Compared to synchrotron X-rays, the single biggest disadvantage of neutrons is that neutron fluxes from reactor, or even accelerator-based sources, are

small. Effectively, this translates into neutron experiments taking much longer to achieve the same signal-to-noise values as ones performed with X-rays. Moreover, the availability of neutron sources is scant compared to the combined availability of the different types of X-ray sources, such as sealed tube and rotating anode X-ray generators, and synchrotron facilities. Nevertheless, as we have seen in a previous section, the many advantageous properties of neutrons, especially those of contrast variation and sensitivity to low Z atoms equally well as heavy ones, make neutrons a highly desirable probe.

1.4.1 Contrast and Structure

Contrast variation has been exploited in several ways. Here, we will only present a broad outline of how it is used to determine the structure and dynamics of biological macromolecules, and leave it to subsequent chapters to provide explicit detail and examples.

The scattering associated with coherent cross-section will have a spatial distribution, which is a function of the distribution of atoms in the sample. The amplitude of the scattered neutron wave is often called the structure factor, and is given by

$$S(\mathbf{Q}) = \sum_i b_i e^{i\mathbf{Q} \cdot \mathbf{r}_i}, \quad (1.13)$$

where the sum is over all atoms in the sample. The measured intensity of neutrons is then proportional to the structure factor squared

$$I(\mathbf{Q}) \propto |S(\mathbf{Q})|^2. \quad (1.14)$$

In a diffraction experiment, resolution is defined as $2\pi/Q_{\max}$, where Q_{\max} is the maximum value of measured amplitude, $|\mathbf{Q}|$. When working at resolutions where individual atoms are not resolved (e.g., $\gtrsim 10$ Å) [18, 20], it is valid to use the concept of a neutron refractive index or scattering length density, $\rho(\mathbf{r})$. Because each nucleus has a different scattering amplitude (ref. Table 1.2), the scattering length density (SLD) is defined as the sum of the coherent scattering lengths over all atoms within a given volume δV , divided by δV [18, 20] or

$$\rho(\mathbf{r})\delta V = \sum_i b_i. \quad (1.15)$$

SLD is the Fourier transform of the structure factor

$$\rho(\mathbf{r}) = \int S(\mathbf{Q}) e^{-i\mathbf{Q} \cdot \mathbf{r}} d\mathbf{Q}. \quad (1.16)$$

In the case of a single crystal, the integral in Eq. 1.16 is over all atoms in the unit cell, and techniques used in X-ray crystallography are entirely applicable. The goal in this case is to determine the scattering length density $\rho(\mathbf{r})$ over

the unit cell, rather than the electron density. Whereas both methods yield the locations of the atoms, \mathbf{r}_i , in the case of neutrons hydrogen atoms with their negative b value (ref. Table 1.2) stand out in much more detail, whereas hydrogen is for all purposes invisible to X-rays.

In general, when solving a crystal structure from diffraction data one has to deal with the well-known *phase problem*. This problem arises from the fact that the structure factor is a complex function, however, the complex part, or the phase, is lost in the measured intensity. A technique devised to resolve the phase problem is *isomorphous replacement*, and involves the addition of an element which effectively changes the neutron or electron density contrast of the crystal. In X-ray crystallography, this usually means the incorporation of heavy atoms such as, Hg into the structure.

In the ideal case, isomorphic replacement does not alter the macromolecule's conformation or the unit cell parameters. This is not always the case when heavy atoms are used to change the sample contrast. On the other hand, the exchange of deuterium for hydrogen, whether in the solvent or explicitly on selected chemical groups, is as nearly perfect isomorphous replacement as possible. The scattering length density of the specific deuterium label, $\rho_l(\mathbf{r})$, can be isolated by taking the measured structure factors from the protonated sample and subtracting them from the deuterated sample as follows

$$\rho_l(\mathbf{r}) = \int [S_D(\mathbf{Q}) - S_H(\mathbf{Q})] e^{-i\mathbf{Q}\cdot\mathbf{r}} d\mathbf{Q}. \quad (1.17)$$

This is analogous to a difference Fourier map in X-ray crystallography, but the possibility of altering the molecule's conformation has been greatly reduced [21].

Where neutron diffraction excels, is the study of samples which cannot be crystallized and display a high degree of disorder, and dispersions of particles in solution. In this case, the benefits of contrast variation are easily seen.

There would be no observable diffraction if particles of uniform scattering length density $\bar{\rho}$ were placed in a solvent where the SLD *matches*, $\rho_s = \bar{\rho}$, and the contrast is zero. Instead, the effective scattering density of a particle whose SLD varies with \mathbf{r} is $\rho(\mathbf{r}) - \rho_s$. For a particle in solution, the measurable contribution of the particle against a backdrop of solvent is given by

$$S_p(\mathbf{r}) = \int [\rho(\mathbf{r}) - \rho_s] e^{i\mathbf{Q}\cdot\mathbf{r}} d\mathbf{r}, \quad (1.18)$$

where the integral is over the the particle volume. The key to finding the particle's structure in solution is to separate $\rho(\mathbf{r})$ into the mean particle density at the match point, $\bar{\rho}_m$, and fluctuations about the mean, $\rho_f(\mathbf{r})$,

$$\rho(\mathbf{r}) = \bar{\rho}_m + \rho_f(\mathbf{r}), \quad (1.19)$$

where $\rho_f(\mathbf{r})$ is normalized by

$$\int \rho_f d\mathbf{r} = 0. \quad (1.20)$$

The contrast in this situation is defined as $\rho_c = \bar{\rho}_m - \rho_s$, which is adjusted by varying the amount of D₂O in the solvent (ref. Sect. 1.4.3). Therefore, contrast variation helps separate particle shape and internal structure contributions to the scattered amplitude. Because scattering from solution averages over all orientations of the particles, modelling of $\rho(\mathbf{r})$ and fitting of $S_p(\mathbf{r})$ are usually performed to fully analyze the data. Although we have neglected the exchange of the molecule's labile H atoms with solvent D atoms, such exchange does take place and will be discussed in the following section.

1.4.2 Contrast and Dynamics

Using neutron spectroscopy to study the dynamics of biological molecules is a comparatively new and developing field. The analysis of inelastic neutron scattering data is complicated and beyond the scope of this introductory chapter. However, the lessons of contrast in structural determination are still applicable. It should be pointed-out that scattering length density is time-dependent, $\rho(\mathbf{r}, t)$, as the atoms are moving, giving rise to inelastic and incoherent scattering, as discussed. In the previous section, we were only concerned with the time-averaged values, $\langle \rho(\mathbf{r}) \rangle$, as we wanted to illustrate the importance of contrast in determining structural information. The dynamic structure factor $S(\mathbf{Q}, \omega)$ is in general more complicated, and is given by

$$G(\mathbf{r}, t) = \frac{1}{N} \int \langle \rho(\mathbf{r}', 0) \rho(\mathbf{r}' - \mathbf{r}, t) \rangle d\mathbf{r}' \quad (1.21)$$

$$S(\mathbf{Q}, \omega) = \frac{1}{2\pi\hbar} \int \int G(\mathbf{r}, t) e^{i(\mathbf{Q} \cdot \mathbf{r} - \omega t)} d\mathbf{r} dt, \quad (1.22)$$

where $G(\mathbf{r}, t)$ is called the time dependent pair correlation function. Clearly, by matching the scattering length density of the solvent to parts of the molecule, one can isolate the relative motions of particular groups or molecules.

1.4.3 Contrast and Biology

It may be seen from Table 1.2 that there is a large difference in the coherent scattering length of deuterium (²H) and hydrogen (¹H), and that the value for the latter, is negative. This arises from a change of phase of the scattered wave with respect to the incident wave, and as explained above, results in a marked difference in scattering power (contrast) between hydrogenous materials containing ²H or ¹H. This has important consequences for the scattering lengths of commonly found biological groups.

Table 1.2 shows the relevant values of scattering cross-section for common biological molecules such as water, and the components of proteins, nucleic

Table 1.2. Bound atom scattering lengths for typical biological chemical groups**A. Amino acids and proteins**

amino acid	exchangeable hydrogen	b_s H ₂ O (10 ⁻¹² cm)	b_s D ₂ O (10 ⁻¹² cm)	b_s deuterated (10 ⁻¹² cm)	volume ^a (Å ³)
glycine	1	1.73	2.77	4.85	71.9
alanine	1	1.65	2.69	6.85	100.5
valine	1	1.48	2.52	10.85	150.8
leucine	1	1.40	2.44	12.85	179.0
isoleucine	1	1.40	2.44	12.85	175.7
phenylalanine	1	4.14	5.18	13.51	201.8
tyrosine	2	4.72	6.80	14.09	205.2
tryptophan	2	6.04	8.12	16.45	239.0
aspartic acid	1	3.85	4.89	8.01	124.2
glutamic acid	1	3.76	4.80	10.01	149.3
serine	2	2.23	4.31	7.43	100.6
threonine	2	2.14	4.23	9.43	127.7
asparagine	3	3.46	6.58	9.70	129.5
glutamine	3	3.37	6.50	11.70	155.9
lysine	4	1.59	5.75	15.12	181.0
arginine	6	3.47	9.72	17.00	211.6
histidine	1.5	4.96	6.52	11.73	163.2
methionine	1	1.76	2.81	11.13	175.4
cystine	2	1.93	4.01	7.14	122.0
proline	0	2.23	2.23	9.52	137.5

B. Nucleotides and nucleic acids

base		exchangeable hydrogen	b_s H ₂ O (10 ⁻¹² cm)	b_s D ₂ O (10 ⁻¹² cm)	b_s deuterated (10 ⁻¹² cm)	volume ^a (Å ³)
adenine	RNA	3	11.24	14.36	22.69	314.0
	DNA	2	10.66	12.74	22.11	
guanine	RNA	4	11.82	15.98	23.27	326.3
	DNA	3	11.24	14.36	22.69	
cytosine	RNA	2	9.27	12.39	20.72	285.6
	DNA	3	8.69	10.77	20.14	
uracil	RNA	2	9.29	11.37	19.70	282.3
thymine	DNA	1	8.62	9.66	21.12	308.7

C. Water

	b_s (10 ⁻¹² cm)	ρ (10 ⁻¹² cm Å ⁻³)
H ₂ O	-0.168	-0.00562
D ₂ O	1.915	0.06404

Table 1.2. *contd.***D. Phosphatidylcholine lipids^b**

	b_s (10^{-12} cm)	ρ (10^{-12} cm \AA^{-3})	b_s deut. (10^{-12} cm)	ρ deut. (10^{-12} cm \AA^{-3})
CH ₃	-0.458	-0.0085	2.67	0.0495
CH ₂	-0.083	-0.0031	2.0	0.0744
headgroup	2.24	0.011	15.67	0.071

^a Values are from Durchschlag and Zipper [22]. Number of exchangeable hydrogen are assumed for pH 7.

^b Values are from Jacrot [19]

acids, and lipids. In nearly all neutron studies some deuteration is used, either for the water in solvation, or of the chemical group itself. When solvating water is replaced by heavy water, some of the hydrogens in the sample will be replaced by deuterium through exchange with the solvent, changing its scattering length density. In general, hydrogen bound to nitrogen or oxygen will be the most likely candidates for exchange. In Table 1.2 this has been taken into account.

Table 1.2 makes two important points. First is that common biological macromolecules have very different scattering lengths. For example, DNA and RNA have considerably larger scattering lengths than proteins, which in turn, are much larger than lipids. This is due to the fact that DNA/RNA have more nitrogen (high positive SLD) and fewer hydrogen (negative SLD) atoms than either, protein or lipid molecules. Lipids have the greatest number of hydrogens per molecule, thanks to their hydrocarbon chains and few exchangeable hydrogens. Thus in any complex, the effects of different molecular species can be highlighted with appropriate contrast matching.

As a simple example, consider the case of a two component particle, containing protein and DNA. In this case, $\rho(\mathbf{r}) = \rho_{\text{pro}}(\mathbf{r}) + \rho_{\text{dna}}(\mathbf{r})$. When $\rho_s = \rho_{\text{pro}}(\mathbf{r})$, the scattering is dominated by the nucleic acid structure, and vice versa.

The second, and probably most important point that can be drawn from Table 1.2 and Fig. 1.4 is that D₂O has a larger scattering length density, and H₂O a lower scattering length density than any of the biological molecules listed. This means that an appropriate mixture of the two solvents can contrast match almost any biological molecule. This is represented graphically in Fig. 1.4, which shows the average scattering length density for model RNA, protein, and lipid membrane systems, as a function of the concentration of D₂O solvent. The points where the line for water crosses the lines for other molecules is called the solvent match point, where the contrast is zero (Fig. 1.4). For DNA and RNA this occurs $\sim 70\%$ D₂O, while for protein, it

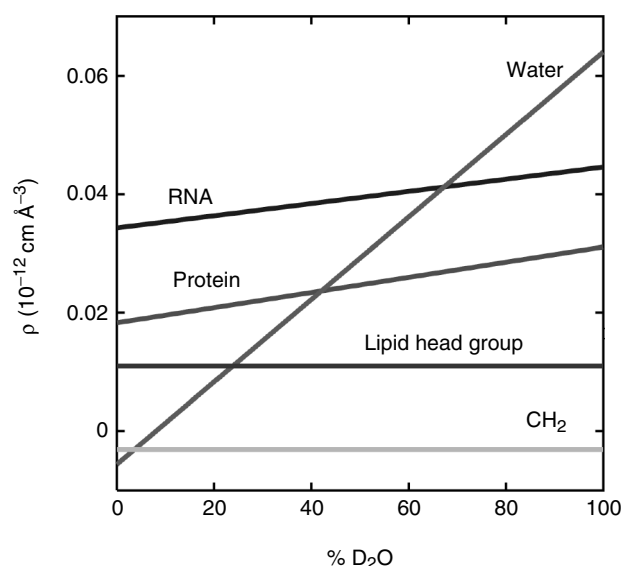


Fig. 1.4. The average scattering length density of typical biological macromolecules, as a function of D_2O concentration in the solvent. The figure is calculated from the data in Table 1.2. The number of exchanged hydrogen is assumed to be complete in 100% D_2O . The figure will depend of the solvent accessible area and specific volume of the molecule, and each case is unique. Note that for water with 8% D_2O , $\rho = 0$. For protein, the line is calculated from the natural abundance of mammalian amino-acid weighed average, and is $\rho = 0.0128 \cdot X + 0.0183$. RNA and DNA (not shown) are less sensitive to H/D exchange; $\rho = 0.0103 \cdot X + 0.0343$ for RNA and $\rho = 0.007 \cdot X + 0.0317$ for DNA

occurs closer to 40%. A more detailed description of the principles underlying contrast variation methods is given in the contribution by J. Krueger et al. (Chapter 8).

1.5 Conclusions

Neutrons are commonly thought of as a tool for hard materials, and for good reason. For the year 2002, published reports involving experiments classified as biological, made up only $\sim 8\%$ of all reports at the Hahn-Meitner Institut (Berlin, Germany) [23], and $\sim 4\%$ at NRC Chalk River [24]. In the 2003 JAERI annual report (Tokai, Japan) $\sim 9\%$ of reports dealt with biology, [25] while only about 6% of the beam time allocated at ILL in 2002 went to proposals in biology [7]. These numbers increase however, if one considers experiments involving so-called bio-materials, which are often classified under soft condensed matter, rather than biology. In this case, around one in eight instrument days at the ILL is devoted to science involving some form of biologically related material [7]. More importantly, the trend with regards to biologically related neutron experiments is upward.

The increasing number of biologically relevant experiments taking place is very much in line with the fact that many neutron facilities are interested in seeing biological problems elucidated with the various neutron scattering techniques available. Presently, biology is an educational outreach tool, that can connect with the public and policy makers in ways that many other sciences cannot. Experiments seen as having some relevance to advances in medicine can be promoted within and beyond the facility. This has had the effect that new instruments devoted to biological sciences such as, the dedicated biological Advanced Neutron Diffractometer/Reflectometer (AND/R) at NIST, and a new 35 m small angle neutron scattering facility at ORNL, are coming online.

The succeeding chapters serve to illustrate the various techniques of neutron diffraction and spectroscopy, in detail. The importance of contrast variation that was introduced in this chapter will serve to demonstrate the broad usefulness that neutron diffraction has in biology.

Acknowledgments

The authors would like to thank V.A. Raghunathan (Raman Research Institute, India) for the many discussions, and M.J. Watson (National Research Council) for providing us with the illustrations used to assemble the various figures.

References

1. J. Chadwick, *Nature* **129**, 312 (1932)
2. J. Chadwick, *Proc. Roy. Soc. A* **136**, 692 (1932)
3. H. Dachs, Principles of neutron diffraction, in *Topics in Current Physics: Neutron Diffraction*, H. Dachs (Eds.) (Springer-Verlag, New York, Berlin, 1978) pp. 1–40
4. W.M. Lomer, G.G. Low, Introductory theory, in *Thermal Neutron Scattering*, P.A. Egelstaff (Eds.) (Academic Press, London, New York, 1965) pp. 1–52
5. B.P. Schoenborn, E. Pitcher, Neutron diffractometers for structural biology at spallation neutron sources, in *Neutron in Biology*, B.P. Schoenborn, R. B. Knott (Eds.) (Plenum Press, New York, 1996) pp. 433–444
6. D.L. Price, K. Sköld, Introduction to neutron scattering, in *Methods of Experimental Physics*, vol. 23 Part A Neutron Scattering, K. Sköld, D.L. Price (Eds.) (Academic Press, Orlando, 1986) pp. 1–97
7. *Institut Laue-Langevin 2002 Annual Report* (ILL, Grenoble, 2003)
8. *NIST Center for Neutron Research 2001 Annual Report* (NIST, Gaithersburg, 2001)
9. G.W. Lynn, M.V. Buchanan, P.D. Butler, L.J. Magid, G.D. Wignall, *J. Appl. Cryst.* **36**, 829 (2003)
10. R. Widreöe, *Arch. Elektrotech.* **21**, 387 (1928)

11. W.K.H. Panofsky, L.W. Alvarez, H. Bradner, H. Gordon, L.C. Marshall, F. Oppenheimer, C. Richman, R. Serber, C. Turner, J.R. Woodyard *Science* **106**, 506 (1947)
12. W.K.H. Panofsky, L.W. Alvarez, H. Bradner, J.V. Franck, H. Gordon, J.D. Gow, L.C. Marshall, F. Oppenheimer, C. Richman, J.R. Woodyard, *Rev. Sci. Instrum.* **26**, 111 (1955)
13. J. Als-Nielsen, D. McMorrow, *Elements of Modern X-Ray Physics* (John Wiley and Sons, England, 2001)
14. C.R. Cantor, P.R. Schimmel, *Biophysical Chemistry Part II: Techniques for the Study of Biological Structure and Function* (W.H. Freeman and Co., San Francisco, 1980)
15. M. Tomita, T. Hasegawa, T. Tsukihara, S. Miyajima, M. Nagao, M. Sato: *J. Biochem. (Tokyo)* **125**, 916 (1999)
16. T. Gutberlet, U. Heinemann, M. Steiner, *Acta Cryst.* **D57**, 349 (2001)
17. G.L. Squires, *Introduction to the Theory of Thermal Neutron Scattering* (Dover Publications, Mineola, New York, 1978)
18. G.D. Wignall, Small angle scattering characterization of polymers, in *Physical Properties of Polymers*, 3rd edn. J.E. Mark (Eds.) (Cambridge University Press, 2004) pp. 424–511
19. B. Jacrot, *Rep. Prog. Phys.* **39**, 911, (1976)
20. G. Zaccai, Application of neutron diffraction to biological problems, in *Topics in Current Physics: Neutron Diffraction*, H. Dachs (Eds.) (Springer-Verlag, New York, Berlin, 1978) pp. 243–269
21. M.C. Weiner, S.H. White, *Biophys. J.* **59**, 174 (1991)
22. H. Durchschlag, P. Zipper: *J. Appl. Cryst.* **30**, 803 (1997)
23. *BENSC experimental reports 2002* (Hahn-Meitner-Institute, Berlin, 2003)
24. *Annual Report 2003 Rapport Annuel* (NRC-CNRC, Canada, 2003)
25. *Progress report on Neutron Scattering Research* (Japan Atomic Energy Research Institute, Tokai, 2004)

Neutron Scattering in Biology

Techniques and Applications

Fitter, J.; Gutberlet, Th.; Katsaras, J. (Eds.)

2006, XXIV, 560 p., Hardcover

ISBN: 978-3-540-29108-4